BBA - Bioenergetics 1867 (2026) 149594

Contents lists available at ScienceDirect

BBA - Bioenergetics

journal homepage: www.elsevier.com/locate/bbabio

Expansion microscopy visualizes the photosystem distribution in *Synechocystis* cells

Peter R. Bos [a,b], Elio Langlois-Legrand [a,c], Emilie Wientjes [a,*]

[a] Laboratory of Biophysics, Wageningen University and Research, 6708, WE, Wageningen, the Netherlands
[b] Molecular Plant Biology, Department of Life Technologies, University of Turku, Turku, 20014, Finland
[c] Laboratoire Reproduction et Développement des Plantes, ENS de Lyon, INRAE, CNRS, UCBL1, INRIA, F-69342, Lyon, France

ARTICLE INFO

Keywords:
Expansion-microscopy
Cyanobacteria
Thylakoid organization
Photosystem

ABSTRACT

Photosynthesis in cyanobacteria relies on light capture by photosystem I (PSI), photosystem II (PSII) and the phycobilisome (PBS). Although these complexes are generally considered to be intermixed within the thylakoid membrane, several studies have suggested the presence of PSI- or PSII/PBS-enriched microdomains that may depend on environmental conditions. Here we applied cryo-Expansion Microscopy (cryo-ExM) to dark-adapted *Synechocystis* sp. PCC 6803 cells and achieved nanoscale resolution of thylakoid compartments and associated protein complexes. Cells were cryofixed, rehydrated at room temperature and physically expanded in a swellable hydrogel. By expanding cells 5.5-fold, we resolved individual thylakoid compartments in intact cells using confocal microscopy. Furthermore, immunolabeling allowed simultaneous localization of PSI, PSII and PBS within the expanded thylakoid network. Overall PSI, PSII, and PBS signals showed similar spatial distributions. However, PBS was excluded from the neck region between dividing cells, while PSI and PSII were present. These results establish cryo-ExM as a powerful method for visualizing cyanobacterial thylakoid membranes and mapping the distribution of key photosynthetic complexes, thereby complementing existing approaches for dissecting the spatial organization of photosynthesis.

1. Introduction

The photosynthetic membrane of cyanobacteria contains Photosystem I (PSI), Photosystem II (PSII), cytochrome *b6f*, and ATP synthase as the major membrane-embedded protein complexes that drive photosynthesis [1]. Together, these complexes perform linear and cyclic electron transport to generate NADPH and ATP, which are subsequently used in CO_2 fixation via the Calvin–Benson cycle [2]. In contrast to higher plants, where the PSI/PSII ratio is typically below one, cyanobacteria like *Synechocystis* sp. PCC 6803 (hereafter *Synechocystis*) and *Synechococcus elongatus* exhibit a higher PSI/PSII ratio ranging from two to five, reflecting a different balance in light harvesting and energy distribution [3–5]. Another fundamental difference is that, in cyanobacteria, photosynthesis and respiration both occur in the thylakoid membrane system, whereas in plants these processes are spatially separated [2,6]. This shared localization requires a distinct organizational structure of the membrane and energy-transfer network.

Instead of the membrane-embedded light-harvesting complexes of plants, cyanobacteria generally employ phycobilisomes (PBSs) as their main antenna system [7]. PBSs are large supramolecular complexes, up to ~70 nm in size, attached to the photosystems or to the thylakoid membrane. PBSs typically consist of a core of allophycocyanin, with rod-like extensions primarily containing phycocyanin and, in some species, additional pigments such as phycoerythrin or phycoerythrocyanin. PBS size and composition are dynamically regulated by light conditions, allowing flexible adjustment of energy transfer [7,8]. Importantly, excitation energy harvested by PBSs can be transferred to both PSI and PSII, depending on the physiological state of the cell, although the extent of PBS-PSI transfer remains under debate [9,10,32,33]. In addition, spillover of excitation energy between PSII and PSI has been suggested to occur in cyanobacteria [11,12].

In higher plants, spillover between PSII and PSI is minimized by the strict spatial separation of photosystems into distinct thylakoid regions: PSII is enriched in grana stacks, while PSI is located primarily in stroma lamellae [34,35]. This heterogeneity is critical for efficient regulation, as disruption of grana stacking leads to growth defects due to impaired light-energy tuning [13,36,37]. Cyanobacteria, by contrast, lack grana and do not display such strict partitioning of PSI and PSII, raising the

* Corresponding author.
E-mail address: Emilie.Wientjes@wur.nl (E. Wientjes).

https://doi.org/10.1016/j.bbabio.2026.149594
Received 29 October 2025; Received in revised form 6 May 2026; Accepted 7 May 2026
Available online 11 May 2026

question of how they maintain photosynthetic efficiency without this structural separation [6,14,15].

An increasing number of studies suggest that cyanobacterial thylakoid membranes may exhibit some degree of spatial heterogeneity through the formation of so-called "microdomains", although the term is used to describe organizational features at different length scales. In some studies, microdomains refer to relatively large membrane regions (approximately 0.5–1.5 μm) enriched in either PSI or PSII, but without the strict lateral segregation observed in plant thylakoids [16]. In contrast, atomic force microscopy studies have described much smaller nanoscale domains, on the order of a few hundred nanometers, consisting of PSI clusters [4,38] or ordered arrays of PSII dimers [39]. Evidence for such domains has been reported based on in vivo and in vitro studies, using biochemical fractionation, atomic force microscopy (AFM), confocal microscopy, or super-resolution imaging [3,16–24]. However, several questions remain regarding the precise nature of these domains and the mechanisms underlying their formation. Firstly, it is still unclear whether microdomains form passively due to membrane dynamics or actively through regulatory processes. Secondly, the effect of isolation is unclear for the in vitro studies or techniques that require isolated membranes. Thirdly, PSI-enriched regions in *S. elongatus* have been observed in either central thylakoids or outer thylakoids, depending on the study [23,24]. Lastly, earlier studies with EM and confocal microscopy in *Synechocystis* did not find evidence for a heterogeneous distribution of PSI and PSII, raising the question of how lower-resolution imaging techniques were able to distinguish those domains in other studies [19,40,41].

Here, we applied cryo-Expansion Microscopy (cryo-ExM) on dark-adapted *Synechocystis* sp. PCC 6803 (hereafter *Synechocystis*) to directly visualize its cellular structure and, in particular, the organization of the photosynthetic membrane. Cryo-ExM combines rapid cryofixation with physical expansion of biological specimens using a swellable hydrogel to achieve nanoscale visualization of cellular organization [25,26]. After vitrification and thawing and rehydration, samples are mildly crosslinked, and anchored to a polyacrylate gel. Subsequent denaturation with SDS at high temperature unfolds proteins and disrupts all noncovalent interactions. As a result, native supramolecular assemblies, including membranes and protein complexes, are not preserved. Instead, spatial information is retained through gel-anchored, denatured polypeptide chains whose relative positions reflect the molecular organization at the time of fixation. Upon isotropic gel swelling, expansion occurs between these anchored biomolecules rather than by stretching covalent bonds or intact membranes, as established in ultrastructure and iterative expansion microscopy approaches [42–45]. Cryo-ExM therefore enables nanoscale mapping of protein distributions within cellular volumes. The method has been shown to preserve positional fidelity at the nm to few tens of nm scale and has been successfully applied to whole cells and organelles, including photosynthetic systems [25,26].

In this cryo-ExM study on dark-adapted *Synechocystis* cells, we labeled PsbA (PSII), PsaC (PSI), and C-phycocyanin (PBS) and resolved the thylakoid organization with an effective ~5.5-fold resolution improvement compared to conventional confocal microscopy. Overall PSI, PSII, and PBS signals showed mainly colocalization, consistent with a largely homogeneous distribution across thylakoid compartments in dark-adapted cells.

2. Material and methods

2.1. Cyanobacterial growth

Synechocystis sp. PCC 6803 and *Synechococcus* elongatus PCC 7942 were grown in 100 mL of BG-11 medium at 30 °C under white light illumination at 30 μmol photons m^{-2} s^{-1} in 250 mL flasks shaken at 160 rpm, containing a stirrer. The original cultures were grown on BG-11 with 1.5% agar plates under the same conditions. Growth of *Synechocystis* sp. PCC 6803 cultures was monitored by measuring optical density at 750 nm throughout the cultivation period. Under the applied illumination conditions of 30 μmol photons m^{-2} s^{-1}, a continuous linear increase in OD_{750} over time was observed, including at low cell densities and up to the sampling point at approximately 320 h after inoculation. No exponential phase was detected under these conditions. This growth behavior is consistent with photon-limited growth, which is expected at low light intensities in phototrophic organisms [46].

2.2. Cryofixation

Cyanobacterial cultures were grown for 13 days after inoculation from a plate. To separate intact from dead cells, the cell suspension was washed twice by centrifuging at 800 ×g for 5 min and resuspended in phosphate-buffered saline. Then, a drop of the cell culture was placed on a 12 mm diameter coverslip that was coated with poly-L-lysine and allowed to sediment for at least 10 min in the dark. Next, we used the Vitrobot Mark IV System by Thermo Fisher to plunge-freeze the slides in liquid ethane according to the cryo-ExM protocol [25,26]. After plunging, the slides were transferred to acetone frozen in liquid nitrogen containing 0.1% paraformaldehyde (PFA) and 0.02% glutaraldehyde (GA) and left overnight on dry ice, where the acetone melted again. The next morning, the tubes were allowed to slowly come to room temperature by removing most of the dry ice and allowing the rest to evaporate. The samples were rehydrated by sequential incubation for 5 min in solutions of 100% ethanol, 95% ethanol (2×), 70% ethanol, 50% ethanol, Milli-Q water, and PBS. The samples were then anchored using a 1.4% PFA, 2.0% acrylamide solution in PBS and incubated for 3 h at 37 °C in a humid environment.

2.3. Expansion microscopy

Next, we applied ExM as before [27,28], with adaptations in the gelation chamber design and gel denaturation. In short, a gel composition of 23% sodium acrylate, 8.9% acrylamide, 0.09% *N,N′*-methylenebisacrylamide in phosphate-buffered saline was made and stored for at least one night at −20 °C. To this gel solution we added a 10% TEMED solution and a 10% APS solution to a final concentration of both of 0.1% to start polymerization. The slide with the fixed and anchored cells was carefully blotted dry without touching the cells. A 25 μL drop of gel solution was placed on a piece of Parafilm on ice and the slide containing the cells was placed on the drop with the cells facing the solution. Polymerization was allowed to occur for 5 min on ice after which the gels were moved to a humid chamber and polymerized further at 37 °C for 90 min.

The gels were removed from the slides with a scalpel and denatured at 95 °C for 90 min in a denaturation buffer (200 mM SDS, 200 mM NaCl and 50 mM Tris base, pH 9.0). The denatured gels were washed at least three times in ultrapure water and left overnight in water to reach full expansion and wash away remaining SDS. A piece of the central part of the gel was cut out and used for staining. A more detailed explanation of this method can be found in Klena's protocol article [25].

2.4. Antibody staining

An overview of the antibodies and fluorophores is given in Table 1. For the antibody staining, we used rabbit polyclonal antibodies targeted against PsbA at 1:200 concentration (Product no: AS05 084) and PsaC at 1:200 (Product no: AS10 939) both purchased from Agrisera (Agrisera AB, Sweden). PsbA was reported to have little off-target binding to proteins, while one extra band was reported for anti-PsaC in *Synechococcus*, as reported on the manufacturer's website. Rabbit anti-C-Phycocyanin antibody was applied at 1:50 (AbBy Fluor® 594) and purchased from Antibody-online (No. ABIN2802262). This antibody was reported to have little off-target binding [47], as was reported for other anti-C-phycocyanin antibodies in *Synechocystis* (CpcA / Anti-C-phycocyanin alpha subunit antibody from PhytoAB, USA).

Table 1
Overview of the antibodies and their associated fluorophores.

Antibody	Host organism	Manufacturer	Dilution	Fluorophore
PsbA (AS05 084)	Rabbit	Agrisera AB	1:200	Secondary antibody or nanobody
PsaC (AS10 939)	Rabbit	Agrisera AB	1:200	ATTO 594 or 647 (conjugation in lab)
AtpB (AS03 030)	Chicken	Agrisera AB	1:100	ATTO 647 (conjugation in lab)
anti-C-Phycocyanin (No. ABIN2802262)	Rabbit	Antibody-online	1:50	AbBy Fluor® 594 (Conjugated by manufacturer)
Anti-rabbit secondary (AB_143165)	Goat	ThermoFisher	1:100	Alexa Fluor™ 488 (Conjugated by manufacturer)
Anti-rabbit secondary nanobody (CTK0102)	Alpaca	ChromoTek GmbH & Proteintech	1:200	Alexa Fluor® 488 (Conjugated by manufacturer)

Anti-PsbA and anti-AtpB (AS05 085, Agrisera AB, Sweden) were conjugated with NHS-ATTO594 or NHS-ATTO647 (ATTO-TEC GmbH, Art. Nr.: AD 594 or 647) by adding 0.2 μL of ATTO dye (dye stock: 10 mg/mL in DMSO) to 15 μL of antibody. The reaction was allowed to proceed for 1 h, and excess dye was removed by using a desalting column (Zeba spin 7 K MWCO Column). The column was washed 4 times with phosphate-buffered saline prior to loading the labeled protein solution. After loading, the column was centrifuged (1500 xg, 1 min) and the eluted fraction was stored in the freezer. The eluted fraction was typically larger than the initial 15 μL of protein, which was taken into account when determining the antibody dilution for staining.

Each antibody staining was diluted in a solution of 0.2% bovine serum albumin in phosphate-buffered saline. Once deposited on the gels, the gels were incubated at 37 °C for 3 h and washed three times with phosphate-buffered saline with 0.1% Tween for 10 min per wash.

Multiplexing was achieved by first staining with anti-PsaC for 3 h at 37 °C followed by two washing steps with phosphate-buffered saline-Tween 0.1%. Then its secondary antibody (Goat anti-Rabbit IgG (H + L) Cross-Adsorbed Secondary Antibody, Alexa Fluor™ 488 (AB_143165), ThermoFisher, or Nano-Secondary® anti-rabbit IgG, recombinant VHH, Alexa Fluor® 488 (CTK0102), ChromoTek GmbH & Proteintech Germany) was applied and left for 1.5 h at 37 °C. After that, anti-C-phycocyanin and anti-PsbA were used simultaneously to avoid extra washing steps with the 3 h incubation time and 37 °C, followed by 2 washing steps with phosphate-buffered saline −0.1% Tween.

2.5. All-protein staining

To create an all-protein staining of the sample, we applied ATTO dyes with an NHS-ester tag. The NHS-ester binds lysine and therefore creates a lysine or protein density staining of the sample [29]. Depending on the other fluorophores present, we used 20 μg/mL N-hydroxysuccinimide (NHS) ester-ATTO-488 (ATTO-TEC GmbH, Art. Nr.: AD 488), ester-ATTO-594 (ATTO-TEC GmbH, Art. Nr.: AD 594) and ester-ATTO-647 (ATTO-TEC GmbH, Art. Nr.: AD 647) in 0.1 M $NaHCO_3$, pH 8.3 with 100 μL per gel in 8-well plate and then incubated for 1.5 h [29].

2.6. Image acquisition

Cut and stained gels were placed in an 8-well plate and left overnight to reduce drift of the gel during imaging. At low laser power, drift was usually negligible, but when higher laser powers were required, the drift became too large to be corrected for. In those instances, gels were placed in a poly-L-lysine-coated 8-well plate.

Samples were imaged using a Leica Stellaris confocal microscope equipped with an HC PL APO CS2 86×/1.20 water objective. This system automatically sets optimized parameters for all dyes and imaging modes. ATTO-488 and Alexa-488 were excited at 501 nm and emission was recorded from 506 to 579 nm, ATTO-594 and Alexa-594 were excited at 590 nm and emission recorded from 595 to 648 nm and ATTO-647 was excited at 646 nm and emission recorded from 660 to 830 nm. Counting mode was used for all channels and 4–8 line accumulations, depending on the intensity of the dyes. If ATTO-594 and ATTO-647 were used simultaneously, crosstalk was prevented by line sequential scanning. ATTO-488 and ATTO-647 were detected in one sequence and ATTO-594 in another. System optimized settings were used for the voxel size, which was typically around 83 × 83 × 356 nm in XYZ. 3D models were created from z-stacks in the Leica LAS X software.

2.7. Image analysis

Image analysis was performed in FIJI [30] and Python3.9.

2.7.1. Peak position

Images of expanded *Synechocystis* cells, stained with anti-PSI, PSII and Phycocyanin antibodies were selected. Slices with the highest intensity in z-stacks were selected by hand. They were analyzed in Python3.9 with the package Scikit-Image [31] in a custom written script to determine the peak position of the three channels. A Gaussian blur and Otsu filter were applied and the X and Y position with the highest number of pixels above the threshold were selected. The intensity profiles along those X and Y points of all channels were taken and smoothed with a Savitsky-Golay filter with a window size of 25 and a 4th order polynomial. Peaks that were at least 0.3 x max intensity, 20 pixels apart and a peak prominence larger than 1.0, were selected. If those peaks in all channels were less than 15 pixels apart, the difference was determined between peak position and the mean peak position. The difference in pixel position was calculated to pre-expanded dimensions by multiplying by the pixel size (83 nm) and divided by the expansion factor (5.5).

3. Results

To identify the localization of the key protein complexes in photosynthesis in *Synechocystis*, we applied cryo-Expansion Microscopy (cryo-ExM). We first cryo-fixed the cells in liquid ethane and after rehydration of the sample, embedded it in a swellable hydrogel [25,26]. The samples were denatured, expanded, and stained with an all-protein NHS ester dye. Little to no background fluorescence was detected from either chlorophyll or phycobilin (Supplemental fig. 1). An expansion factor of 5.5 was sufficient to resolve individual thylakoid compartments, each consisting of two membrane layers and the enclosed lumen (Fig. 1). In addition to the thylakoid membranes, the carboxysomes were clearly visible as bright spheres in the center of the cell. An intensity plot showed the repeat distance of thylakoid compartments to be roughly 91 ± 20 nm apart, but on occasion, we could distinguish compartments that were less than 60 nm apart in pre-expanded dimensions. The average separation distance is somewhat larger than the 78 nm reported before in *Synechococcus elongatus* [20] and considerably larger than the 62 nm reported for *Synechocystis* with neutron scattering [40]. However, with our expansion factor we are unable to distinguish thylakoid layers that are closer than 60 nm, which may lead to an overestimation of the average repeat distance.

We localized PSI, PSII and the PBS using antibodies against PsaC, PsbA and phycocyanin, respectively. Overlay of the all-protein NHS-ester staining with the antibody labeling demonstrated that all three antibodies specifically localized to the thylakoid membrane (Fig. 2). Other proteindense regions, like the carboxysomes [48], were hardly

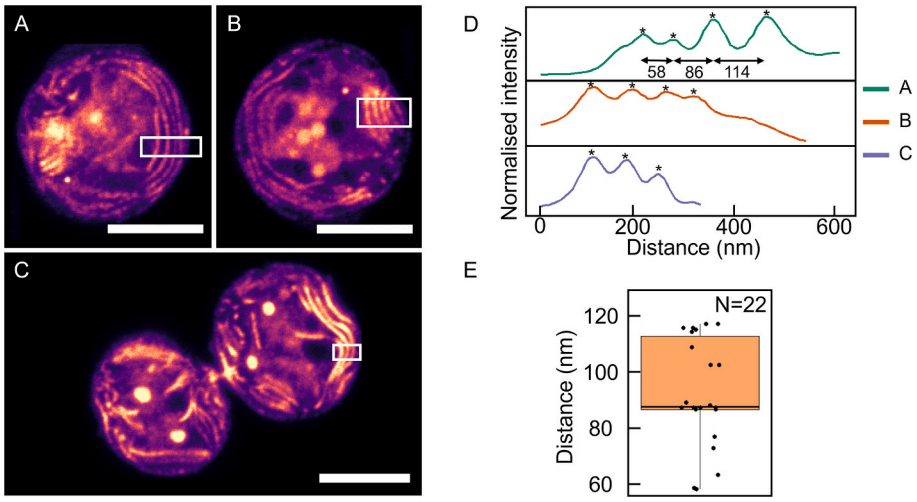

Fig. 1. A-C) Micrographs of expanded *Synechocystis* cell, stained with an all-protein staining. Scale bars represent 1 μm in pre-expanded dimension. White boxes indicate regions from which the profiles are plotted in D. Peak positions of the thylakoid membrane are indicated by asterisks and for A the differences between the peaks are indicated in nm, pre-expanded dimensions. E) Peak spacings from D and other images, plotted in a boxplot. 95th percentile and 5th percentile are indicated by whiskers, the box represents 25th to 75th percentile and the central line indicates the median.

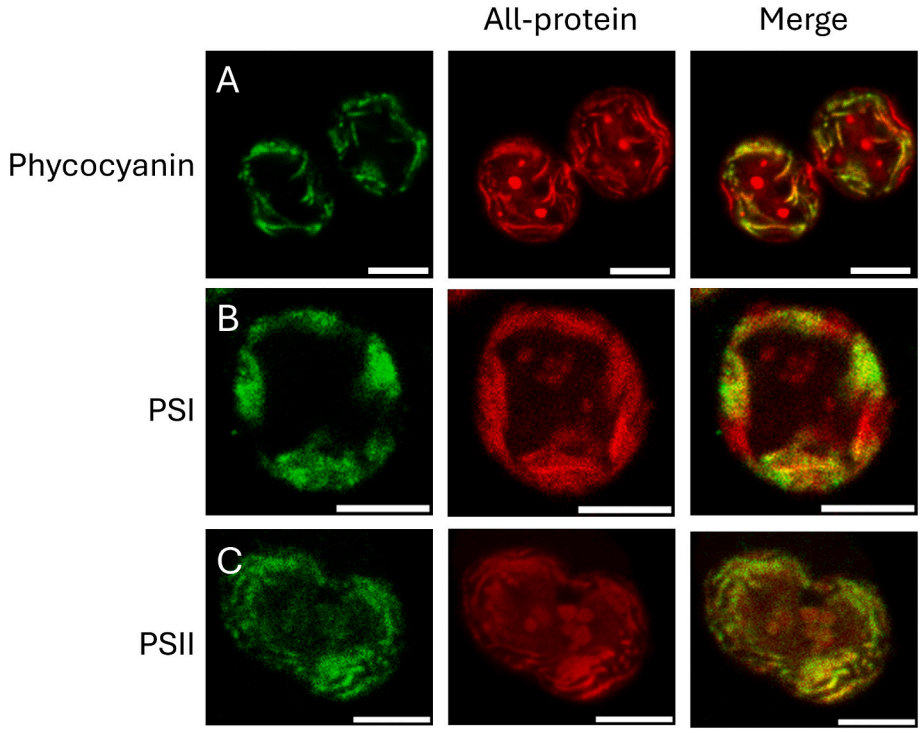

Fig. 2. A-C) Representative micrographs of expanded *Synechocystis* cells, immunolabeled (green) and all-protein stained (red). Scale bars represent 1 μm in pre-expanded dimensions. (For interpretation of the references to colour in this figure legend, the reader is referred to the web version of this article.)

visible in the antibody channels. Negative control using only the secondary antibody showed no signal (Supplemental Fig. 2). Moreover, we localized ATP synthase with an AtpB antibody and found it to localize to both the thylakoid membrane and plasma membrane (SI Fig. 3). Surprisingly, in some images, only staining of the plasma membrane was observed and hardly any thylakoid localization. However, the antibody also localized to regions outside the cell in a dotted manner, potentially indicating aggregation of the antibody.

Next, we localized PSI, PSII and PBS in the same sample. Merging of the micrographs indicated a large extent of overlap between the three antibody signals (Fig. 3 and Supplemental Fig. 4). Radial heterogeneity was assessed by drawing profiles over the entire cell, thereby capturing the thylakoid regions on either side of the cell (Fig. 4). Small differences in the ratios of PSI, PSII and PBS were detected. To check whether either of these protein complexes localized preferentially to the center or periphery of the cell, we determined their peak position. Specifically, we determined the peak intensity of PSI, PSII, and PBS within individual cells (SI Fig. 5) and calculated the deviation of each complex from the mean peak position. This analysis revealed a small (20 nm on average, while the resolution is >60 nm), but significant difference between the peak positions of PSI and PBS, with PSI concentrated slightly more toward the cell center and PBS somewhat more to the periphery.

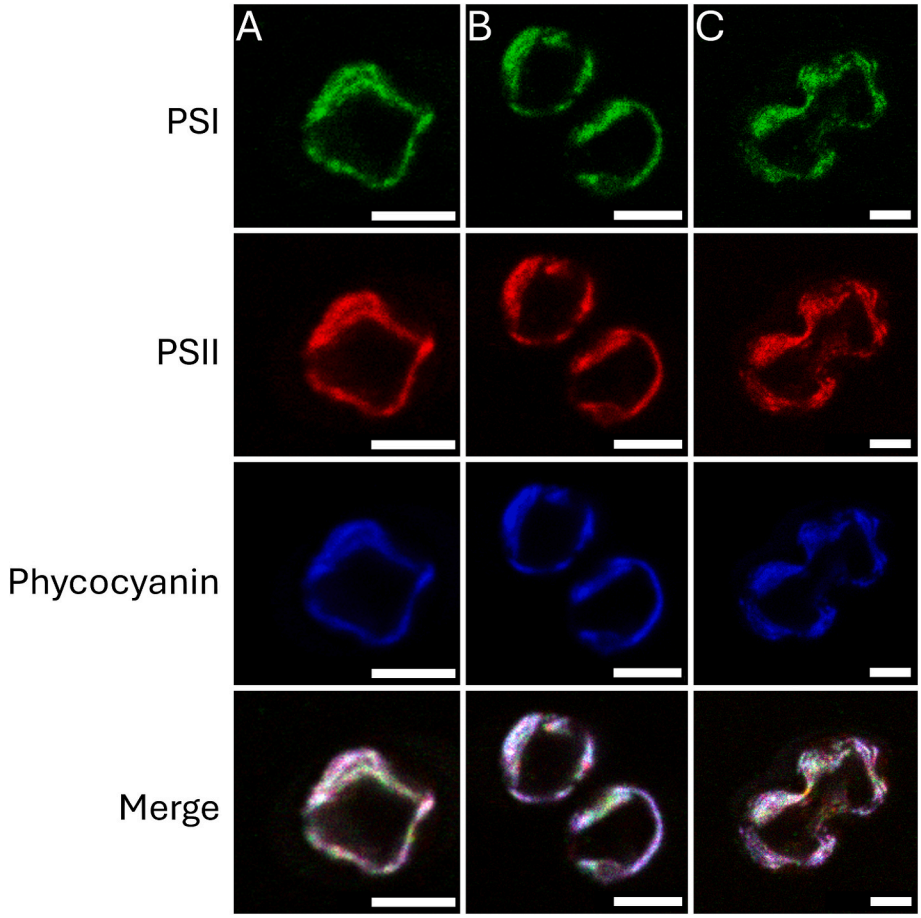

Fig. 3. Micrographs of expanded, immunolabeled *Synechocystis* cells showing PSI (anti-PsaC, green), PSII (anti-PsbA, red), and PBS (anti-C-phycocyanin, blue). Merged images are shown in the bottom panels. Scale bars represent 1 μm in pre-expanded dimensions. (For interpretation of the references to colour in this figure legend, the reader is referred to the web version of this article.)

Next, intensity profiles were extracted along selected thylakoid membrane regions and normalized to allow comparison of spatial distribution patterns between PSI, PSII, and PBS signals (Fig. 4). Overall, the normalized intensity profiles showed broadly similar spatial trends for all three antibodies along the membrane, indicating a high degree of co-localization. In most regions, PSI and PSII profiles overlapped, while PBS, which exhibited the highest overall fluorescence intensity, followed a comparable general distribution but showed occasional local deviations in relative intensity along the thylakoid membrane.

Some apparent differences in signal ratios between channels were observed; however, these should be interpreted with caution. PSI displayed the lowest signal intensity and consequently the lowest signal to noise ratio, which may contribute to increased variability in the normalized PSI profiles. Because normalization was performed independently for each channel to enable comparison of spatial patterns, relative differences in low intensity signals may be accentuated. Taken together, the data indicate a largely overlapping spatial organization of PSI, PSII, and PBS along the thylakoid membrane, while some variations in relative distribution may be present. It must be noted that these intensity profiles are the average of several thylakoid membrane layers combined, as our resolution did not allow for resolving individual layers.

In most images, we detected colocalization of PSI, PSII and PBS. However, exceptions were found during division (Fig. 5). Several cells had nearly completed binary fission but remained connected by a narrow tube. The connecting region contained thylakoids with PSI and PSII, yet it showed a decreased intensity of the phycocyanin-PBS antibody. In the 'neck' between dividing cells, the thylakoid layers were closer together than elsewhere in the cell in the all-protein stained cells (Fig. 1C and 2A), potentially excluding the large PBS from these parts.

In conclusion, we detected a large degree of overlap between PSI, PSII or PBS in the thylakoid membrane of *Synechocystis* with cryo-ExM, except for some confined regions of cells at a stage of division.

4. Discussion

4.1. Exploration of Cryo-ExM methodology

Cryo-ExM proved highly effective for *Synechocystis* cells without requiring cell wall-degrading enzymes. With an expansion factor of 5.5, thylakoid layers became clearly resolved after NHS-all protein staining. Attempts with chemical fixation as performed in earlier ExM studies on photosynthetic membranes [27,28] occasionally yielded expanded cells, but cells sometimes lost their round shape, suggesting anisotropic expansion. Moreover, immunolabeling resulted in less intense fluorescence. Results with *Synechococcus elongatus* PCC 7942 yielded some well-expanded cells, but all gels also contained some unexpanded cells or cells that lost their rigid rod-like shape (SI fig. 6). Moreover, PSI and PSII antibody staining were generally faint. The approach of cryo-ExM seems promising for more cyanobacterial species, but could require optimization of the fixation, expansion and staining protocols.

The antibodies used in this study, anti-PsaC, anti-PsbA, and anti-phycocyanin, all localized to thylakoid membranes in *Synechocystis*, and not to other protein-dense regions such as carboxysomes. Among them, anti-phycocyanin gave the strongest signal. Anti-AtpB (ATP synthase β subunit) localized to the plasma membrane and to a lesser extent to the thylakoid membrane (SI Fig. 3). The antibody used here

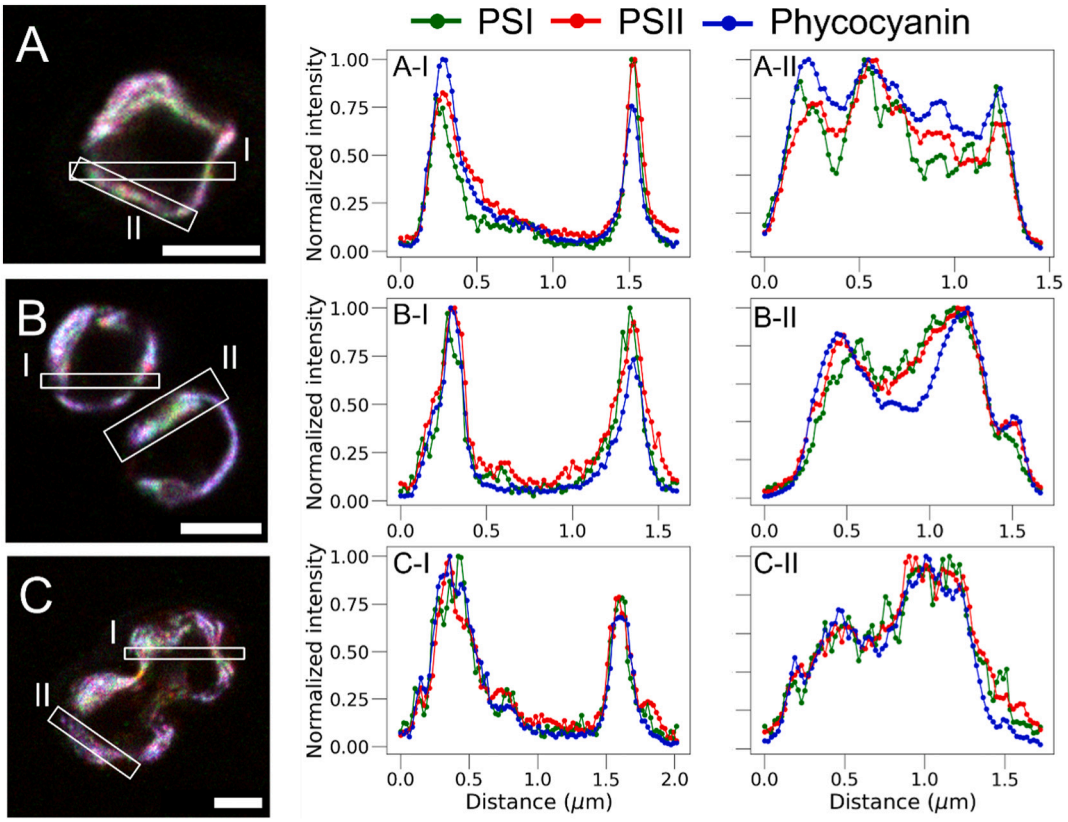

Fig. 4. Micrographs of expanded and immunolabeled *Synechocystis* cells showing merged signals of PSI (green), PSII (red), and PBS (anti-C-phycocyanin, blue). Images correspond to those shown in Fig. 3. White boxes indicate regions used to extract intensity profiles. Profiles were normalized to the minimum and maximum intensity values, and distances are shown in pre-expanded dimensions. Scale bars represent 1 μm in pre-expanded dimensions. (For interpretation of the references to colour in this figure legend, the reader is referred to the web version of this article.)

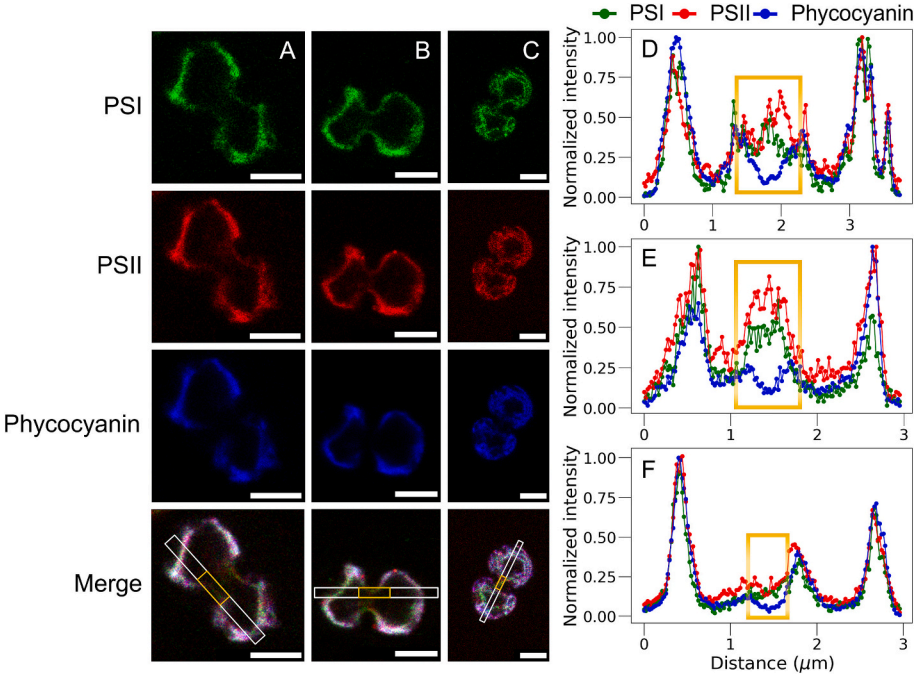

Fig. 5. Expanded, immunolabeled *Synechocystis* cells and corresponding intensity profiles for PSI (anti-PsaC, green), PSII (anti-PsbA, red), and PBS (anti-C-phycocyanin, blue). In the merged images (bottom panels), white boxes indicate regions from which intensity profiles were extracted (D-F). Panel D corresponds to image A, E to B, and F to C. Profiles were normalized to the minimum and maximum intensity values, and distances are shown in pre-expanded dimensions. The yellow box marks the connecting region between dividing cells, where reduced phycocyanin signal was observed. Scale bars represent 1 μm in pre-expanded dimensions. (For interpretation of the references to colour in this figure legend, the reader is referred to the web version of this article.)

recognizes the beta subunit of F-ATP synthases that are present in the thylakoid membrane of plants and the thylakoid and plasma membrane of bacteria, which explains the localization to both domains. However, the antibody showed a patchy pattern both on thylakoid regions inside the cell and in regions outside the cell. Although this pattern might reflect microdomains of ATP synthase, as previously observed with eGFP labeling [3], it could also result from imperfect recognition or clustering of the antibody. To elucidate the localization of ATP-synthase in cyanobacteria in more detail, different ATP synthase antibodies or a genetically encoded ATP synthase tag can be used.

Together, these findings highlight cryo-ExM as a promising tool for visualizing cyanobacterial cells and protein localization by immunolabeling. The method may be applicable to other cyanobacteria, with or without protocol modification. For species with a more complex cell wall, incorporation of cell wall–digesting enzymes may be necessary. Beyond antibody labeling, cryo-ExM could be combined with genetically introduced epitopes (e.g. GFP tags recognized by anti-GFP antibodies). Such approaches open new possibilities for studying protein targeting pathways or the balance between photosynthesis and respiration, in cyanobacteria.

4.2. Image analysis considerations

Most microscopy studies identify microdomains by comparing fluorescence intensity ratios across channels [16,18,21,22]. While this approach can be effective in systems with stable labeling and uniform signal levels, it was not suitable for our workflow. Our extensive sample preparation (fixation, denaturation, gelation, and washing) can lead to partial epitope loss, and antibody labeling efficiency varied between samples. Consequently, applying a uniform threshold across images was not feasible, while per-image thresholding would have introduced bias. For this reason, threshold-dependent metrics such as the Manders coefficient were not appropriate.

We also evaluated the Pearson correlation coefficient (PCC), which measures the covariance of pixel intensities between channels. However, PCC was not informative for our data. PSI, PSII, and PBS all localize to the same thylakoid membrane system, and the effective resolution after expansion does not allow individual thylakoid layers to be resolved. As a result, fluorescence signals from all channels largely overlap and exhibit similar spatial distributions, leading to uniformly high PCC values. Importantly, PCC reflects global intensity similarity rather than spatial organization and is insensitive to local differences in protein ratios. Therefore, high PCC values in this context primarily indicate that the proteins occupy the same general cellular region and cannot be used to assess the presence or absence of microdomains. In addition, PCC values can be influenced by differences in antibody signal intensity and by the use of a common cell mask, further limiting its interpretability.

We therefore created intensity plots over a whole cell, or along the thylakoid membrane to compare intensity of the three photosynthetic complexes (Fig. 4). To ease comparison, we normalized the profiles individually to their minimum and maximum intensity. The trend in intensity over the thylakoid membrane was similar for all three antibodies, but for some, the ratio between the intensities was variable. For example, the offset in Fig. 4 A-II is largely caused by normalization to an outlier in the PSI intensity, therefore shifting the rest of the profile down. The other characteristics of the PBS profile are well followed by the PSI profile. However, due to the low signal to noise level of the PSI antibody, we are cautious in interpreting the presence of microdomains. Large-scale absences of one photosynthetic complex seem to be absent in our data, but our data is insufficiently clear to draw conclusions on the presence of the smaller 'nanodomains' of PSI that have been proposed.

The intensity profiles of the antibodies over a cell did not indicate large deviations in PSI, PSII and PBS ratios, but provided information on their positioning. Smoothed intensity profiles across the center of *Synechocystis* cells (SI Fig. 5) revealed that PSI tended to peak slightly closer to the cell interior than PBS (phycocyanin). However, this shift was not consistent across individual cells and remained below the effective imaging resolution (mean difference ~ 20 nm versus ~60 nm resolution), becoming statistically significant only due to the sample size ($N = 54$). Moreover, the apparent shift can be explained by differences in signal-to-noise ratios between channels: PSI labeling produced weaker fluorescence, allowing residual background to extend further into the cell interior, whereas the stronger PBS signal was more effectively confined by filtering. Future work should examine whether these profiles change under light conditions known to alter PSI–PSII distribution [18,20].

4.3. Absence of phycocyanin in cell division regions

The strongest evidence for regions with ratiometric alterations in the photosynthetic complexes were regions in which thylakoid layers were in close proximity. At connecting regions of dividing cells, PSI and PSII were present, but PBS (phycocyanin) was absent. Given the large size of PBS (~40 nm height), steric hindrance in confined thylakoid areas may exclude intact PBS complexes [7]. It is possible that PBSs are remodeled into smaller subunits that remain associated with PSI or PSII, which could be tested using antibodies against PBS core proteins.

4.4. In summary

Several studies using fractionation, AFM, and microscopy have reported a heterogeneous separation of PSI and PSII into microdomains [3,16–24]. In contrast to plants, this separation in cyanobacteria is not strict, but manifests itself as stable variations in ratios of photosystems. Some studies report relatively large membrane regions of approximately 0.5 to 1.5 μm described as being enriched in either PSI or PSII-PBS complexes [16]. Here we explored the use of cryo-ExM to investigate the distribution of light-harvesting complexes in dark-adapted *Synechosystis* cells. PSI, PSII, and PBS signals showed a high degree of overlap throughout the thylakoid compartments. At the same time, regions displaying variations in the relative abundance of the three antibody signals were observed. It remains unclear whether these differences reflect true spatial variation in protein distribution or are influenced by differences in labelling efficiency and resulting signal intensity. Further optimization of antibody staining and signal normalization strategies may help resolve this in future studies. Notably, PBS signals were consistently excluded from the connecting regions at the division site in dividing cells, indicating a localized redistribution of the light-harvesting antenna system during cell division.

CRediT authorship contribution statement

Peter R. Bos: Writing – original draft, Visualization, Supervision, Methodology, Investigation, Formal analysis, Data curation, Conceptualization. **Elio Langlois-Legrand:** Writing – review & editing, Visualization, Investigation, Data curation. **Emilie Wientjes:** Writing – review & editing, Supervision, Funding acquisition, Conceptualization.

Declaration of competing interest

The authors declare the following financial interests/personal relationships which may be considered as potential competing interests: Emilie Wientjes reports financial support was provided by Dutch Research Council. If there are other authors, they declare that they have no known competing financial interests or personal relationships that could have appeared to influence the work reported in this paper.

Acknowledgements

This work was supported by the Dutch Organization for Scientific Research (NWO) via a Vidi grant (VI. Vidi 192.042 to E.W.).

Appendix A. Supplementary data

Supplementary data to this article can be found online at https://doi.org/10.1016/j.bbabio.2026.149594.

Data availability

Data will be made available on request.

References

[1] S. Rexroth, M.M. Nowaczyk, M. Rögner, Cyanobacterial photosynthesis: the light reactions, in: Modern Topics in the Phototrophic Prokaryotes: Metabolism, Bioenergetics, and Omics, Springer, 2017, pp. 163–191.

[2] D.J. Lea-Smith, P. Bombelli, R. Vasudevan, C.J. Howe, Photosynthetic, respiratory and extracellular electron transport pathways in cyanobacteria, Biochim. Biophys. Acta - Bioenerg. 1857 (3) (2016) 247–255.

[3] S. Casella, F. Huang, D. Mason, G.-Y. Zhao, G.N. Johnson, C.W. Mullineaux, L.-N. Liu, Dissecting the native architecture and dynamics of cyanobacterial photosynthetic machinery, Mol. Plant 10 (11) (2017) 1434–1448.

[4] C. MacGregor-Chatwin, M. Sener, S.F.H. Barnett, A. Hitchcock, M.C. Barnhart-Dailey, K. Maghlaoui, J. Barber, J.A. Timlin, K. Schulten, C.N. Hunter, Lateral segregation of photosystem I in cyanobacterial thylakoids, Plant Cell 29 (5) (2017) 1119–1136.

[5] V. Moore, W. Vermaas, Functional consequences of modification of the photosystem I/photosystem II ratio in the cyanobacterium Synechocystis sp. PCC 6803, J. Bacteriol. 206 (5) (2024) e00454-23.

[6] C.W. Mullineaux, Function and evolution of grana, Trends Plant Sci. 10 (11) (2005) 521–525.

[7] N. Adir, S. Bar-Zvi, D. Harris, The amazing phycobilisome, Biochim. Biophys. Acta - Bioenerg. 1861 (4) (2020) 148047.

[8] D.M. Kehoe, A. Gutu, Responding to color: the regulation of complementary chromatic adaptation, Annu. Rev. Plant Biol. 57 (1) (2006) 127–150.

[9] P. Akhtar, A. Biswas, F. Balog-Vig, I. Domonkos, L. Kovács, P.H. Lambrev, Trimeric photosystem I facilitates energy transfer from phycobilisomes in Synechocystis sp. PCC 6803, Plant Physiol. 189 (2) (2022) 827–838.

[10] I.H.M. van Stokkum, D.M. Niedzwiedzki, P. Akhtar, A. Biswas, P.H. Lambrev, H. Liu, Cyanobacteria dynamically regulate phycobilisome-to-photosystem excitation energy transfer, IScience 28 (6) (2025).

[11] W. Ma, L. Chen, L. Wei, Q. Wang, Excitation energy transfer between photosystems in the cyanobacterium Synechocystis 6803, JOL 128 (3) (2008) 546–548.

[12] Y. Ueno, S. Aikawa, K. Niwa, T. Abe, A. Murakami, A. Kondo, S. Akimoto, Variety in excitation energy transfer processes from phycobilisomes to photosystems I and II, Photosynth. Res. 133 (1) (2017) 235–243.

[13] H.-W. Trissl, C. Wilhelm, Why do thylakoid membranes from higher plants form grana stacks? Trends Biochem. Sci. 18 (11) (1993) 415–419.

[14] C.W. Mullineaux, Excitation energy transfer from phycobilisomes to photosystem I in a cyanobacterium, Biochim. Biophys. Acta - Bioenerg. 1100 (3) (1992) 285–292.

[15] C.W. Mullineaux, A.R. Holzwarth, Effect of photosystem II reaction centre closure on fluorescence decay kinetics in a cyanobacterium, Biochim. Biophys. Acta - Bioenerg. 1183 (2) (1993) 345–351.

[16] A. Straśková, G. Steinbach, G. Konert, E. Kotabová, J. Komenda, M. Tichý, R. Kaňa, Pigment-protein complexes are organized into stable microdomains in cyanobacterial thylakoids, Biochim. Biophys. Acta - Bioenerg. 1860 (12) (2019) 148053.

[17] R. Agarwal, A. Matros, M. Melzer, H.-P. Mock, J.K. Sainis, Heterogeneity in thylakoid membrane proteome of Synechocystis 6803, J. Proteome 73 (5) (2010) 976–991.

[18] M. Canonico, G. Konert, R. Kaňa, Plasticity of cyanobacterial thylakoid microdomains under variable light conditions, Front. Plant Sci. 11 (2020) 586543.

[19] A.M. Collins, M. Liberton, H.D.T. Jones, O.F. Garcia, H.B. Pakrasi, J.A. Timlin, Photosynthetic pigment localization and thylakoid membrane morphology are altered in Synechocystis 6803 phycobilisome mutants, Plant Physiol. 158 (4) (2012) 1600–1609.

[20] T. Huokko, T. Ni, G.F. Dykes, D.M. Simpson, P. Brownridge, F.D. Conradi, R. J. Beynon, P.J. Nixon, C.W. Mullineaux, P. Zhang, Probing the biogenesis pathway and dynamics of thylakoid membranes, Nat. Commun. 12 (1) (2021) 3475.

[21] R. Kaňa, B. Šedivá, O. Prášil, Microdomains heterogeneity in the thylakoid membrane proteins visualized by super-resolution microscopy, Photosynthetica 61 (4) (2023) 483.

[22] R. Kaňa, M. Eichner, A. Gall, C. Ilioaia, Spatial heterogeneity in the photobiology of phototrophs—questions and methods, Front. Photobiol. 2 (2024) 1384522.

[23] D.M. Sherman, T.A. Troyan, L.A. Sherman, Localization of membrane proteins in the cyanobacterium Synechococcus sp. PCC7942 (radial asymmetry in the photosynthetic complexes), Plant Physiol. 106 (1) (1994) 251–262.

[24] W.F.J. Vermaas, J.A. Timlin, H.D.T. Jones, M.B. Sinclair, L.T. Nieman, S. W. Hamad, D.K. Melgaard, D.M. Haaland, In vivo hyperspectral confocal fluorescence imaging to determine pigment localization and distribution in cyanobacterial cells, Proc. Natl. Acad. Sci. 105 (10) (2008) 4050–4055.

[25] N. Klena, G. Maltinti, U. Batman, G. Pigino, P. Guichard, V. Hamel, An in-depth guide to the ultrastructural expansion microscopy (U-ExM) of chlamydomonas reinhardtii, Bio-Protocol 13 (17) (2023) e4792.

[26] M.H. Laporte, N. Klena, V. Hamel, P. Guichard, Visualizing the native cellular organization by coupling cryofixation with expansion microscopy (Cryo-ExM), Nat. Methods 19 (2) (2022) 216–222.

[27] J. Berentsen, P.R. Bos, E. Wientjes, Expansion microscopy reveals thylakoid organisation alterations due to genetic mutations and far-red light acclimation, Biochim. Biophys. Acta - Bioenerg. 1866 (3) (2025) 149552.

[28] P.R. Bos, J. Berentsen, E. Wientjes, Expansion microscopy resolves the thylakoid structure of spinach, Plant Physiol. 194 (1) (2024) 347–358.

[29] O. M'Saad, J. Bewersdorf, Light microscopy of proteins in their ultrastructural context, Nat. Commun. 11 (1) (2020) 3850.

[30] J. Schindelin, I. Arganda-Carreras, E. Frise, V. Kaynig, M. Longair, T. Pietzsch, S. Preibisch, C. Rueden, S. Saalfeld, B. Schmid, Fiji: an open-source platform for biological-image analysis, Nat. Methods 9 (7) (2012) 676–682.

[31] S. Van der Walt, J.L. Schönberger, J. Nunez-Iglesias, F. Boulogne, J.D. Warner, N. Yager, E. Gouillart, T. Yu, scikit-image: image processing in Python, PeerJ 2 (2014) e453.

[32] R.R. Choubeh, E. Wientjes, P.C. Struik, D. Kirilovsky, H. Van Amerongen, State transitions in the cyanobacterium Synechococcus elongatus 7942 involve reversible quenching of the photosystem II core, Biochimica et Biophysica Acta (BBA)-Bioenergetics 1859 (10) (2018) 1059–1066.

[33] V. Chukhutsina, L. Bersanini, E.M. Aro, H. Van Amerongen, Cyanobacterial light-harvesting phycobilisomes uncouple from photosystem I during dark-to-light transitions, Sci. Rep. 5 (1) (2015) 14193.

[34] B. Andersson, J.M. Anderson, Lateral heterogeneity in the distribution of chlorophyll-protein complexes of the thylakoid membranes of spinach chloroplasts, Biochimica et Biophysica Acta (BBA)-Bioenergetics 593 (2) (1980) 427–440.

[35] J.P. Dekker, E.J. Boekema, Supramolecular organization of thylakoid membrane proteins in green plants, Biochimica et Biophysica Acta (BBA)-Bioenergetics 1706 (1–2) (2005) 12–39.

[36] U. Armbruster, M. Labs, M. Pribil, S. Viola, W. Xu, M. Scharfenberg, D. Leister, Arabidopsis CURVATURE THYLAKOID1 proteins modify THYLAKOID architecture by inducing membrane curvature, Plant Cell 25 (7) (2013) 2661–2678.

[37] M. Pribil, O. Sandoval-Ibáñez, X. Wenteng, A. Sharma, M. Labs, Q. Liu, C. Galgenmüller, T. Schneider, M. Wessels, S. Matsubara, S. Jansson, G. Wanner, D. Leister, Fine-tuning of photosynthesis requires CURVATURE THYLAKOID1-mediated THYLAKOID plasticity, Plant Physiol. 176 (3) (March, 2018) 2351–2364, https://doi.org/10.1104/pp.17.00863Pribil, M., Sandoval-Ibáñez, O., Xu, W., Sharma, A., Labs, M., Liu, Q., ... & Leister, D. (2018). Fine-tuning of photosynthesis requires CURVATURE THYLAKOID1-mediated thylakoid plasticity. Plant Physiology, 176(3), 2351-2364.

[38] C. MacGregor-Chatwin, D.J. Nürnberg, P.J. Jackson, C. Vasilev, A. Hitchcock, M.-Y. Ho, G. Shen, C.J. Gisriel, W.H.J. Wood, M. Mahbub, V.M. Selinger, M. P. Johnson, M.J. Dickman, A.W. Rutherford, D.A. Bryant, C.N. Hunter, Changes in supramolecular organization of cyanobacterial thylakoid membrane complexes in response to far-red light photoacclimation, Sci. Adv. 8 (2022) eabj4437, https://doi.org/10.1126/sciadv.abj4437.

[39] L.-S. Zhao, T. Huokko, S. Wilson, D.M. Simpson, Q. Wang, A.V. Ruban, C. W. Mullineaux, Y.-Z. Zhang, L.-N. Liu, Structural variability, coordination and adaptation of a native photosynthetic machinery, Nat. Plants 6 (2020) 869–882, https://doi.org/10.1038/s41477-020-0694-3.

[40] M. Liberton, L.E. Page, W.B. O'Dell, H. O'Neill, E. Mamontov, V.S. Urban, H. B. Pakrasi, Organization and flexibility of cyanobacterial thylakoid membranes examined by neutron scattering, J. Biol. Chem. 288 (5) (2013) 3632–3640.

[41] Van De Meene, M.F. Hohmann-Marriott, W.F. Vermaas, R.W. Roberson, The three-dimensional structure of the cyanobacterium Synechocystis sp. PCC 6803, Arch. Microbiol. 184 (5) (2006) 259–270.

[42] V. Louvel, R. Haase, O. Mercey, M.H. Laporte, T. Eloy, É. Baudrier, D. Fortun, D. Soldati-Favre, V. Hamel, P. Guichard, iU-ExM: nanoscopy of organelles and tissues with iterative ultrastructure expansion microscopy, Nat. Commun. 14 (1) (2023) 7893.

[43] A.H. Shaib, A.A. Chouaib, R. Chowdhury, J. Altendorf, D. Mihaylov, C. Zhang, D. Krah, V. Imani, R.K.W. Spencer, S.V. Georgiev, N. Mougios, M. Monga, S. Reshetniak, T. Mimoso, H. Chen, P. Fatehbasharzad, D. Crzan, K.-A. Saal, M. M. Alawieh, N. Alawar, J. Eilts, J. Kang, A. Soleimani, M. Müller, C. Pape, L. Alvarez, Claudia Trenkwalder, B. Mollenhauer, T.F. Outeiro, S. Köster, J. Preobraschenski, U. Becherer, T. Moser, E.S. Boyden, A. Radu Aricescu, M. Sauer, F. Opazo, S.O. Rizzoli, One-step nanoscale expansion microscopy reveals individual protein shapes, Nat. Biotechnol. 43 (9) (2025) 1539–1547.

[44] S. Truckenbrodt, M. Maidorn, D. Crzan, H. Wildhagen, S. Kabatas, S.O. Rizzoli, X10 expansion microscopy enables 25-nm resolution on conventional microscopes, The EMBO Reports 19 (9) (2018) EMBR201845836.

[45] S. Truckenbrodt, C. Sommer, S.O. Rizzoli, J.G. Danzl, A practical guide to optimization in X10 expansion microscopy, Nat. Protoc. 14 (3) (2019) 832–863.

[46] L. Martínez, A. Morán, A.I. García, Effect of light on Synechocystis sp. and modelling of its growth rate as a response to average irradiance, J. Appl. Phycol. 24 (1) (2012) 125–134.

[47] E.N. Geh, D. Ghosh, M. McKell, de la Cruz, G. Stelma, J.A. Bernstein, Identification of Microcystis aeruginosa peptides responsible for allergic sensitization and characterization of functional interactions between cyanobacterial toxins and immunogenic peptides, Environ. Health Perspect. 123 (11) (2015) 1159.

[48] J.S. MacCready, A.G. Vecchiarelli, Positioning the model bacterial organelle, the carboxysome, MBio 12 (3) (2021) 10–1128.